Consideration of Interface Damping in Shrouded Mistuned Turbine Blades

F. Schreyer, J. Gross, P. Reuss, University of Stuttgart; M. Junge, H. Schoenenborn, MTU Aero Engines

Abstract Running turbines are exposed to high mechanical load. Due to gas excitations the structure can vibrate with high oscillation amplitudes which can damage the turbine blades. Mistuning can additionally lead to high local stresses which must be taken into account in the turbine design process. Introducing damping due to friction in the interface of shrouded turbines can be used to decrease this oscillation amplitudes. The computation of full turbine finite-element models with nonlinear coupling forces causes high computational costs. As a consequence, Component Mode Synthesis methods are used to reduce the number of DOFs of each blade substructure. Mistuning of the blades can now be applied in modal space. Coupling of the mistuned substructures is done by nonlinear interface forces which have to be included in the substructuring formulation. The resulting reduced and mistuned system with nonlinear coupling forces is solved with a Harmonic Balance Method such that the effect of mistuning and interface damping can be studied very efficiently.

Keywords: Turbine, Mistuning, Interface Damping, Component Mode Synthesis, Harmonic Balance Method

1 Introduction

Calculating the steady state response of turbine blades is an important task during the design process of turbines. To analyze the oscillation of randomly mistuned turbine blades stochastic analysis must be done. In general, this requires many calculations and therefore a very fast numeric routine is desirable. If nonlinear contacts are considered, the calculation is very time expensive. In this contribution a fast approximation for the nonlinear contact on shrouded blades is presented using the Harmonic Balance Method (HBM). Additionally, a Component Mode Synthesis (CMS) to reduce the linear substructures is used to decrease the calculation time to a minimum.
A small benchmark model is considered in order to show the approach and illustrate numeric results. In Fig. 1 the components as well as the assembly of the used FE-model are shown.

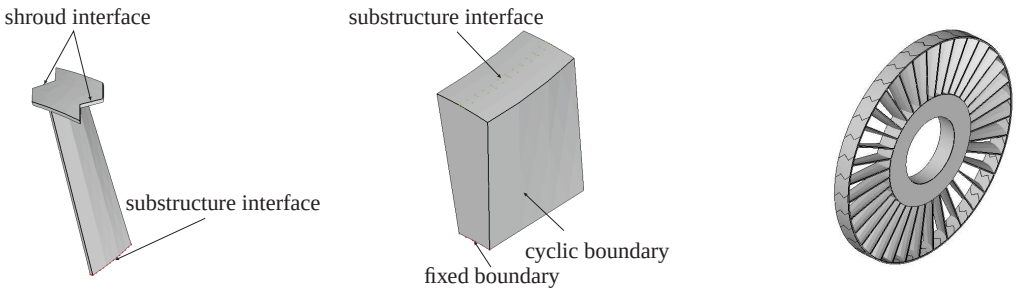

Fig. 1 Blade-, disk-components and assembly of the finite-element model.

F. Schreyer, J. Gross, P. Reuss
Institute of Applied and Experimental Mechanics, University of Stuttgart, Pfaffenwaldring 9, 70550 Stuttgart
e-mail: {schreyer,gross,reuss}@iam.uni-stuttgart.de

This paper is organized as follows. In Chapter 2 the reduction and adjacent assembly of the substructures are described in detail. Chapter 3 is addressed to the used mistuning formulation. The coupling method applied to the shroud interfaces is demonstrated in Chapter 4. Subsequently, the Harmonic Balance Method is shortly reviewed in Chapter 5 and Chapter 6 is dedicated to the obtained results. The paper closes with a brief conclusion.

2 Component Mode Synthesis of the turbine

Finite-element models of turbine blades have a large number of degrees of freedom (DOFs). By using a model reduction method the order of the system can be reduced to save computational costs. Following the approach presented in [1, 2, 3], a CMS is used to reduce the disk and blade segments separately, and assemble to the full system hereafter.

2.1 Reduction of the blade

The DOFs of the blade are reduced using the Craig-Bampton method. Interface DOFs are kept in the physical domain, while free DOFs are replaced by a combination of fixed interface modes and constraint modes. Therefore, the mass and stiffness matrix, $\boldsymbol{M}^b$ and $\boldsymbol{K}^b$ must be partitioned into free (f) and interface (i) DOFs. The upper index denotes the blade (b). Note, that here the interface (i) consists of the shroud interface (i_{shr}) and the segment interface of the disk (i_d).

$$\underbrace{\begin{bmatrix} \boldsymbol{M}^b_{\mathrm{ff}} & \boldsymbol{M}^b_{\mathrm{fi}} \\ \boldsymbol{M}^b_{\mathrm{if}} & \boldsymbol{M}^b_{\mathrm{ii}} \end{bmatrix}}_{\boldsymbol{M}^b} \begin{bmatrix} \ddot{\boldsymbol{x}}^b_{\mathrm{f}} \\ \ddot{\boldsymbol{x}}^b_{\mathrm{i}} \end{bmatrix} + \underbrace{\begin{bmatrix} \boldsymbol{K}^b_{\mathrm{ff}} & \boldsymbol{K}^b_{\mathrm{fi}} \\ \boldsymbol{K}^b_{\mathrm{if}} & \boldsymbol{K}^b_{\mathrm{ii}} \end{bmatrix}}_{\boldsymbol{K}^b} \begin{bmatrix} \boldsymbol{x}^b_{\mathrm{f}} \\ \boldsymbol{x}^b_{\mathrm{i}} \end{bmatrix} = \begin{bmatrix} \boldsymbol{0} \\ \boldsymbol{f}^b_{\mathrm{i}} \end{bmatrix}, \quad \text{with} \quad \boldsymbol{x}^b_{\mathrm{i}} = \begin{bmatrix} \boldsymbol{x}^b_{\mathrm{i_d}} \\ \boldsymbol{x}^b_{\mathrm{i_{shr}}} \end{bmatrix}. \tag{1}$$

Consequently, to determine the fixed interface modes, the eigenvalue problem

$$\left(\boldsymbol{K}^b_{\mathrm{ff}} - \omega^2_{\mathrm{j}} \boldsymbol{M}^b_{\mathrm{ff}}\right) \boldsymbol{\phi}^b_{\mathrm{j}} = \boldsymbol{0} \tag{2}$$

must be solved. The dynamics of the reduced system is defined by the first n eigenvectors $\boldsymbol{\Phi}^b = \left[\boldsymbol{\phi}^b_1, \ldots, \boldsymbol{\phi}^b_{\mathrm{n}}\right]$. The number of required eigenvectors to achieve accurate solutions depends on the analyzed frequency range. Additionally, the reduction base $\boldsymbol{\Theta}$ is enriched by the constraint modes so that it can be written as

$$\begin{bmatrix} \boldsymbol{x}^b_{\mathrm{f}} \\ \boldsymbol{x}^b_{\mathrm{i}} \end{bmatrix} = \begin{bmatrix} \boldsymbol{\Phi}^b & -\boldsymbol{K}^{b-1}_{\mathrm{ff}} \boldsymbol{K}^b_{\mathrm{fi}} \\ \boldsymbol{0} & \boldsymbol{I} \end{bmatrix} \begin{bmatrix} \boldsymbol{p}^b \\ \boldsymbol{x}^b_{\mathrm{i}} \end{bmatrix} = \boldsymbol{\Theta} \begin{bmatrix} \boldsymbol{p}^b \\ \boldsymbol{x}^b_{\mathrm{i}} \end{bmatrix}. \tag{3}$$

The reduced matrices are obtained by multiplying the reduction base to the system matrices

$$\boldsymbol{M}^b_{\mathrm{red}} = \boldsymbol{\Theta}^{\mathrm{T}} \boldsymbol{M}^b \boldsymbol{\Theta}, \quad \boldsymbol{K}^b_{\mathrm{red}} = \boldsymbol{\Theta}^{\mathrm{T}} \boldsymbol{K}^b \boldsymbol{\Theta}. \tag{4}$$

In order to expand the blade to a complete system of Ns segments, the single blade matrices , Eq. (4) can be arranged in a block diagonal form. If the system matrices are represented in the Cartesian system the coordinates of n-th blade must be transformed by a rotation matrix T_n, containing a multiple of the sector angle,

$$\bar{\boldsymbol{M}}^b_{\mathrm{red}} = \underset{n=1(1)N_s}{blkdiag}(\boldsymbol{T}^T_{\mathrm{n}} \boldsymbol{M}^b_{\mathrm{red,n}} \boldsymbol{T}_{\mathrm{n}}) \quad \bar{\boldsymbol{K}}^b_{\mathrm{red}} = \underset{n=1(1)N_s}{blkdiag}(\boldsymbol{T}^T_{\mathrm{n}} \boldsymbol{K}^b_{\mathrm{red,n}} \boldsymbol{T}_{\mathrm{n}}). \tag{5}$$

The bar symbol constitutes global coordinates of all n blades.

2.2 Reduction and cyclic transformation of the disk

For the reduction of the disk cyclic symmetry can be used. The cyclic symmetric boundary condition can be applied by the matrix transformation

$$\begin{bmatrix} \boldsymbol{x}_{\mathrm{f}} \\ \boldsymbol{x}_{\mathrm{i_{cyc},r}} \\ \boldsymbol{x}_{\mathrm{i_{cyc},l}} \end{bmatrix} = \begin{bmatrix} \boldsymbol{I} & \boldsymbol{0} \\ \boldsymbol{0} & \boldsymbol{I} \\ \boldsymbol{0} & \boldsymbol{T}e^{-i\alpha h} \end{bmatrix} \begin{bmatrix} \boldsymbol{x}_{\mathrm{f}} \\ \boldsymbol{x}_{\mathrm{i_{cyc},r}} \end{bmatrix}, \tag{6}$$

which forces the left boundary $\boldsymbol{x}_{\mathrm{i_{cyc},l}}$ to oscillate phase shifted with respect to the right one $\boldsymbol{x}_{\mathrm{i_{cyc},r}}$. This phase shift is defined by the harmonic index h, the sector angle α. The matrix $\boldsymbol{T}$ describes the geometrical rotation from the left to the right boundary. To capture the global disk dynamics, all indices $h = 0(1)N_s - 1$ must be taken into account. The dynamic behavior of the disk can, thus, be expressed in a block diagonal form

$$\tilde{\boldsymbol{M}}^d = \underset{h=0(1)N_s-1}{blkdiag}\ (\tilde{\boldsymbol{M}}^d_{\mathrm{h}}), \quad \tilde{\boldsymbol{K}}^d = \underset{h=0(1)N_s-1}{blkdiag}\ (\tilde{\boldsymbol{K}}^d_{\mathrm{h}}), \tag{7}$$

where each submatrix represents one harmonic index. The harmonic indices are decoupled by definition [1], and therefore the Craig-Bampton reduction can be performed for each harmonic index separately. Consequently, after the reduction the disk is described by modal and cyclic coordinates which results to a much smaller number of DOFs,

$$\tilde{\boldsymbol{M}}^d_{\mathrm{red}} = \underset{n=0(1)N_s-1}{blkdiag}\ (\boldsymbol{\Theta}^T_{\mathrm{h}}\tilde{\boldsymbol{M}}^d_{\mathrm{h}}\boldsymbol{\Theta}_{\mathrm{h}}), \quad \tilde{\boldsymbol{K}}^d_{\mathrm{red}} = \underset{n=0(1)N_s-1}{blkdiag}\ (\boldsymbol{\Theta}^T_{\mathrm{h}}\tilde{\boldsymbol{K}}^d_{\mathrm{h}}\boldsymbol{\Theta}_{\mathrm{h}}). \tag{8}$$

2.3 Assembly and Interface Reduction

After the modal reduction of the single segment components and their adjacent expansion to full systems of N_s sectors, the coupling of the substructure interface can be performed. The interface DOFs of the blades are still in physical domain, while the interface DOFs of the disk are expressed in cyclic coordinates. Therefore, to couple the interface DOFs of the blades are transformed using the Fourier matrix $\bar{\boldsymbol{F}}$

$$\bar{\boldsymbol{x}}^b_{\mathrm{i_d}} = \begin{bmatrix} \boldsymbol{x}^b_{\mathrm{i_d}1} & \cdots & \boldsymbol{x}^d_{\mathrm{i_d N_s}} \end{bmatrix}^T = \bar{\boldsymbol{F}}\tilde{\boldsymbol{x}}^d \tag{9}$$

which is defined as

$$\bar{\boldsymbol{F}} = \boldsymbol{I} \otimes \boldsymbol{F} \quad \text{with} \quad \boldsymbol{F}(kk,ll) = \frac{1}{N_s}e^{i(kk-1)(ll-1)\alpha}. \tag{10}$$

The blades and disk can now be assembled by the assembly matrix $\boldsymbol{T}_{\mathrm{cms}}$, which transforms and couples the substructure interface DOFs,

$$\begin{bmatrix} \tilde{\boldsymbol{p}}^d_{\mathrm{f}} \\ \tilde{\boldsymbol{x}}^d_{\mathrm{i}} \\ \bar{\boldsymbol{p}}^b_{\mathrm{f}} \\ \bar{\boldsymbol{x}}^b_{\mathrm{i}} \\ \bar{\boldsymbol{x}}^b_{\mathrm{r}} \end{bmatrix} = \underbrace{\begin{bmatrix} \boldsymbol{I} & \boldsymbol{0} & \boldsymbol{0} & \boldsymbol{0} \\ \boldsymbol{0} & \boldsymbol{I} & \boldsymbol{0} & \boldsymbol{0} \\ \boldsymbol{0} & \boldsymbol{0} & \boldsymbol{I} & \boldsymbol{0} \\ \boldsymbol{0} & \bar{\boldsymbol{F}} & \boldsymbol{0} & \boldsymbol{0} \\ \boldsymbol{0} & \boldsymbol{0} & \boldsymbol{0} & \boldsymbol{I} \end{bmatrix}}_{\boldsymbol{T}_{\mathrm{cms}}} \begin{bmatrix} \tilde{\boldsymbol{p}}^d_{\mathrm{f}} \\ \tilde{\boldsymbol{x}}_{\mathrm{i}} \\ \bar{\boldsymbol{p}}^b_{\mathrm{f}} \\ \bar{\boldsymbol{x}}^b_{\mathrm{r}} \end{bmatrix}. \tag{11}$$

Note, that in this case only conforming meshes of the substructure interfaces are considered, [10]. The mass matrix $\boldsymbol{M}_{\mathrm{cms}}$ of the assembly, can be written as

$$\boldsymbol{M}_{\mathrm{cms}} = \boldsymbol{T}^T_{\mathrm{cms}} \begin{bmatrix} \tilde{\boldsymbol{M}}^d_{\mathrm{red}} & \boldsymbol{0} \\ \boldsymbol{0} & \bar{\boldsymbol{M}}^b_{\mathrm{red}} \end{bmatrix} \boldsymbol{T}_{\mathrm{cms}} = \begin{bmatrix} \tilde{\boldsymbol{M}}^d_{\mathrm{red,ff}} & \tilde{\boldsymbol{M}}^d_{\mathrm{red,fi}} & \boldsymbol{0} & \boldsymbol{0} \\ \tilde{\boldsymbol{M}}^d_{\mathrm{red,if}} & \tilde{\boldsymbol{M}}_{\mathrm{red,ii}} & \bar{\boldsymbol{M}}^b_{\mathrm{red,if}}\bar{\boldsymbol{F}} & \bar{\boldsymbol{M}}^b_{\mathrm{red,ir}}\bar{\boldsymbol{F}} \\ \tilde{\boldsymbol{0}} & \bar{\boldsymbol{F}}^T\bar{\boldsymbol{M}}^b_{\mathrm{red,fi}} & \bar{\boldsymbol{M}}^b_{\mathrm{red,ff}} & \bar{\boldsymbol{M}}^b_{\mathrm{red,fr}} \\ \boldsymbol{0} & \bar{\boldsymbol{F}}^T\bar{\boldsymbol{M}}^b_{\mathrm{red,ri}} & \bar{\boldsymbol{M}}^b_{\mathrm{red,rf}} & \bar{\boldsymbol{M}}^b_{\mathrm{red,rr}} \end{bmatrix}. \tag{12}$$

The assembly stiffness matrix $\boldsymbol{K}_{\text{cms}}$ is defined accordingly. The size of the system is still dominated by the large number of cyclic interface DOFs, which can be further reduced by an interface reduction. The modal reduction basis of the interface is obtained by solving the eigenvalue problem of the interface partitions from Eq. (12).

$$\left(\tilde{\boldsymbol{K}}_{\text{red,ii}} - \boldsymbol{\omega}_{\text{ii}}^2 \tilde{\boldsymbol{M}}_{\text{red,ii}}\right) \tilde{\boldsymbol{\Phi}}_{\text{ii}} = \boldsymbol{0} \tag{13}$$

The eigenvectors of the interface $\tilde{\boldsymbol{\Phi}}_{\text{ii}}$ span the same subspace as the constraint modes of the global interface between disk and blades, which can be truncated by keeping only the eigenvectors associated with the lowest k eigenfrequencies $\boldsymbol{\omega}_{\text{k,ii}}$. The transformation for the new set coordinates can be formulated as

$$\begin{bmatrix} \tilde{\boldsymbol{p}}_{\text{f}}^{d} \\ \tilde{\boldsymbol{x}}_{\text{i}} \\ \overline{\boldsymbol{p}}_{\text{f}}^{b} \\ \overline{\boldsymbol{x}}_{\text{r}}^{b} \end{bmatrix} = \underbrace{\begin{bmatrix} \boldsymbol{I} & \boldsymbol{0} & \boldsymbol{0} & \boldsymbol{0} \\ \boldsymbol{0} & \tilde{\boldsymbol{\Phi}}_{\text{k,ii}} & \boldsymbol{0} & \boldsymbol{0} \\ \boldsymbol{0} & \boldsymbol{0} & \boldsymbol{I} & \boldsymbol{0} \\ \boldsymbol{0} & \boldsymbol{0} & \boldsymbol{0} & \boldsymbol{I} \end{bmatrix}}_{\boldsymbol{\Theta}_{\text{i}}} \begin{bmatrix} \tilde{\boldsymbol{p}}_{\text{f}}^{d} \\ \tilde{\boldsymbol{p}}_{\text{i}} \\ \overline{\boldsymbol{p}}_{\text{f}}^{b} \\ \overline{\boldsymbol{x}}_{\text{r}}^{b} \end{bmatrix}, \tag{14}$$

and the assembled system matrices can be rewritten as

$$\boldsymbol{M}_{\text{cms,red}} = \boldsymbol{\Theta}_{\text{i}}^{T} \boldsymbol{M}_{\text{cms}} \boldsymbol{\Theta}_{\text{i}}, \qquad \boldsymbol{K}_{\text{cms,red}} = \boldsymbol{\Theta}_{\text{i}}^{T} \boldsymbol{K}_{\text{cms}} \boldsymbol{\Theta}_{\text{i}}, \tag{15}$$

where $\boldsymbol{\Theta}_{\text{i}}$ represents the interface reduction matrix.The assembled system can be further reduced by a final Craig-Bampton reduction of the system matrices, substituting the individual blade and disk modes by a set of global modes. The shroud-coupling DOFs are kept in the physical domain.

3 Mistuning

The perfect cyclic symmetry of a bladed disk is destroyed, when mistuning is present. Especially blades are highly affected by variations of the manufacturing process as well as operational wear which leads to significant disturbance in the spread of vibrational energy in the system. Assuming only a variance of the Young's modulus, a nondimensional mistuning parameter can be defined as

$$\delta_{\text{n}} = \frac{\omega_{\text{n,mist}}^2 - \omega_{\text{nom}}^2}{\omega_{\text{nom}}^2}. \tag{16}$$

The nominal eigenfrequency of the tuned blade is denoted by ω_{nom}^2, and $\omega_{\text{n,mist}}^2$ describes the mistuned eigenfrequency of the n-th blade. Furthermore, proportional mistuning is assumed, that means the percentage deviation of natural frequencies is the same for all modes, [5]. The mistuning deviations are small compared to nominal properties in the modal domain, i.e., $|\delta| << 1$, and it is hypothesized that the mode shapes are the same for a mistuned blade as for the tuned one.
Note, that for a validation the mistuning parameters are preferably obtained from measured cantilevered modes. However, when sliding condition is applied, the shroud constraint modes also need to be mistuned to describe the motion of the blade more accurately, [5]. Therefore, the mistuning projection requires two sets of modes. On the one hand $\boldsymbol{U}_{\text{shr}}^{b}$, including the fixed interface modes $\boldsymbol{\Phi}^{b}$ in combination with the shroud constraint modes, which were already obtained in Eq. (3). On the other hand the fixed-interface normal modes $\boldsymbol{\Phi}_{\text{cnt}}^{b}$, which in contrast to $\boldsymbol{\Phi}^{b}$ are obtained by neglecting the shroud coupling. The $\boldsymbol{\Phi}_{\text{cnt}}^{b}$ are associated with the mistuning parameters δ_{n} and therefore are used to transfer the mistuned stiffness matrix into physical domain. The modal stiffness deviation matrix $\Delta\boldsymbol{K}_{\text{n,mist}}^{b}$ is obtained by adjacent projecting on $\boldsymbol{U}_{\text{shr}}^{b}$, which leads to

$$\Delta\boldsymbol{K}_{\text{mist,n}}^{b} = {\boldsymbol{U}_{\text{shr}}^{b}}^{T} \boldsymbol{M}^{b} \boldsymbol{\Phi}_{\text{cnt}}^{b} \delta_{\text{n}} {\boldsymbol{\Phi}_{\text{cnt}}^{b}}^{T} \boldsymbol{K}_{\text{red,n}}^{b} \boldsymbol{U}_{\text{shr}}^{b}, \tag{17}$$

with

$$\boldsymbol{U}_{\text{shr}}^{b} = \begin{bmatrix} \boldsymbol{\Phi}^{b} & -\boldsymbol{K}_{\text{ff}}^{b} \boldsymbol{K}_{\text{fi}_{\text{shr}}}^{b} \\ \boldsymbol{0} & \boldsymbol{I} \end{bmatrix}, \quad \boldsymbol{\Phi}_{\text{cnt}}^{b} = \begin{bmatrix} \boldsymbol{\Phi}_{\text{cnt}} \\ \boldsymbol{0} \end{bmatrix}. \tag{18}$$

Note, that here mistuning is applied to the partitions of the free DOFs as well as the shroud DOFs. The modal mistuned stiffness matrix of each blade is then given by

$$\boldsymbol{K}_{\text{mist,n}}^{b} = \Delta\boldsymbol{K}_{\text{mist,n}}^{b} + \boldsymbol{K}_{\text{red,n}}^{b}. \tag{19}$$

4 Coupling of the shrouds

Due to the reduction method described above the interface DOFs of the shroud remain in physical coordinates. Node-to-node contact model can be applied there directly. In order to achieve fast calculations a simple Jenkins model with the assumption of a constant normal force is used [6]. Therefore, the normal directions of the contact faces are rigidly connected to each other and the tangential relative displacements are used to calculate the friction forces [7]. It should be noted that any kind of contact could be considered here. For reasons of clarity the procedure is explained by taking a general mechanical system representation. For the results presented in Chapter 6 the described procedure is applied on the reduced matrices derived in the previous sections. The set of assembled system equations can be written as

$$\boldsymbol{M}\ddot{\boldsymbol{x}} + \boldsymbol{D}\dot{\boldsymbol{x}} + \boldsymbol{K}\boldsymbol{x} = \boldsymbol{f} + \boldsymbol{g} \tag{20}$$

where $\boldsymbol{f}$ is the vector of external forces and $\boldsymbol{g}$ the vector of contact forces between the substructures. Due to the matching meshes of the shroud interfaces the relative displacement vector $\boldsymbol{u}$ of the contact nodes can be expressed with a signed boolean matrix $\boldsymbol{B}$. In order to apply different types of coupling to the normal and tangential direction, $\boldsymbol{B}$ can be partitioned into $\boldsymbol{B}_\mathrm{p}$ for the 'perfect' coupling in normal and $\boldsymbol{B}_\mathrm{f}$ for the tangential 'flexible' coupling [8]

$$\begin{bmatrix} \boldsymbol{u}_\mathrm{N} \\ \boldsymbol{u}_\mathrm{T} \end{bmatrix} = \begin{bmatrix} \boldsymbol{B}_\mathrm{p} \\ \boldsymbol{B}_\mathrm{f} \end{bmatrix} \boldsymbol{x}. \tag{21}$$

Note that in general a coordinate transformation is needed to obtain the normal and tangential directions of the interfaces. Considering the rigid coupling, the forces are eliminated as unknowns using the interface equilibrium. According to Eq. (21) the compatibility condition can be expressed by

$$\boldsymbol{B}_\mathrm{p}\boldsymbol{x} = \boldsymbol{0} \tag{22}$$

and the force equilibrium condition is given by

$$\boldsymbol{L}_\mathrm{p}^T \boldsymbol{g} = \boldsymbol{0}. \tag{23}$$

The matrix $\boldsymbol{L}_\mathrm{p}$ locates the unique set of DOFs $\boldsymbol{q}$ in the whole DOFs vector. Due to the fact that the compatibility condition must be fulfilled for all $\boldsymbol{q}$ it can be shown that $\boldsymbol{L}_\mathrm{p}$ must be the null space of $\boldsymbol{B}_\mathrm{p}$ and vice versa,

$$\boldsymbol{B}_\mathrm{p}\boldsymbol{x} = \boldsymbol{B}_\mathrm{p}\boldsymbol{L}_\mathrm{p}\boldsymbol{q} = \boldsymbol{0} \quad \forall \boldsymbol{q} \qquad \Longrightarrow \qquad \boldsymbol{L}_\mathrm{p} = null(\boldsymbol{B}_\mathrm{p}). \tag{24}$$

Consequently, a rigid coupling between the normal displacements of the shroud interfaces can be achieved by transforming the equation of motion with the matrix $\boldsymbol{L}_\mathrm{p}$. When nonlinear coupling forces in tangential direction are present, the compatibility condition no longer equals zero. Following [8] the tangential interface forces can be defined using Lagrange multipliers

$$\boldsymbol{g} = -\boldsymbol{B}_\mathrm{f}^T \boldsymbol{\lambda}, \tag{25}$$

where $\boldsymbol{\lambda}$ denotes the force intensities. Due to the characteristic of the Boolean matrix $\boldsymbol{B}_\mathrm{f}$ the equilibrium condition always is satisfied. Additionally, the Boolean matrix defines the relative displacements as

$$\boldsymbol{u}_\mathrm{T} = \boldsymbol{B}_\mathrm{f}\boldsymbol{x}. \tag{26}$$

These relative displacements are then used to calculate the nonlinear force vector $\boldsymbol{\lambda}$ by considering the Jenkins model properties [7]. With Eq. (20) and Eq. (25) all nonlinear forces can be built into the FE-system.

The described method can be used to couple the shrouds and different interface conditions can be applied:

- free shrouds: no coupling is applied
- fixed shrouds: all DOFs are fixed
- linear sliding contact: only normal directions of nodes are rigidly coupled, all the others are free.
- nonlinear friction contact: normal direction is rigidly coupled and nonlinear forces are present in tangential plane

The final equation of the reduced and coupled system, which is to be solved can now be expressed as

$$\mathbb{M}\ddot{\boldsymbol{q}} + \mathbb{D}\dot{\boldsymbol{q}} + \mathbb{K}\boldsymbol{q} + \boldsymbol{F}_{\mathrm{nl}}(\dot{\boldsymbol{q}}, \boldsymbol{q}) = \boldsymbol{f}_{\mathrm{exc}}, \tag{27}$$

where

$$\begin{gathered}
\mathbb{M} = \boldsymbol{L}_{\mathrm{p}}^T \boldsymbol{M} \boldsymbol{L}_{\mathrm{p}}, \quad \mathbb{D} = \boldsymbol{L}_{\mathrm{p}}^T \boldsymbol{D} \boldsymbol{L}_{\mathrm{p}}, \quad \mathbb{K} = \boldsymbol{L}_{\mathrm{p}}^T \boldsymbol{K} \boldsymbol{L}_{\mathrm{p}}, \\
\boldsymbol{F}_{\mathrm{nl}} = \boldsymbol{L}_{\mathrm{p}}^T \boldsymbol{B}_{\mathrm{f}}^T \begin{bmatrix} \boldsymbol{F}_{\mathrm{nl,1,x}} \\ \boldsymbol{F}_{\mathrm{nl,1,y}} \\ \vdots \\ \boldsymbol{F}_{\mathrm{nl,N_s,x}} \\ \boldsymbol{F}_{\mathrm{nl,N_s,y}} \end{bmatrix} \quad \text{and} \quad \boldsymbol{f}_{\mathrm{exc}} = \boldsymbol{L}_{\mathrm{p}}^T \boldsymbol{f}.
\end{gathered} \tag{28}$$

5 Harmonic Balance Method

To reach higher accuracy, the solution of the nonlinear Eq. (28) can also be approximated by the Higher Harmonic Balance method. The mandatory transformation of the system equations into the frequency domain may introduce complex valued amplitudes in the displacement and force vectors [7], which are denoted by the hat symbol. The mathematical representation of the system equations in frequency domain is given by

$$\begin{bmatrix} \mathbb{H}_{\mathrm{lin},0} & \boldsymbol{0} & \cdots & \boldsymbol{0} \\ \boldsymbol{0} & \mathbb{H}_{\mathrm{lin},1} & \boldsymbol{0} & \vdots \\ \vdots & \boldsymbol{0} & \ddots & \boldsymbol{0} \\ \boldsymbol{0} & \cdots & \boldsymbol{0} & \mathbb{H}_{\mathrm{lin},\mathrm{m_h}} \end{bmatrix} \begin{bmatrix} \hat{\boldsymbol{q}}_0 \\ \hat{\boldsymbol{q}}_1 \\ \vdots \\ \hat{\boldsymbol{q}}_{\mathrm{m_h}} \end{bmatrix} = \begin{bmatrix} \hat{\boldsymbol{f}}_{\mathrm{exc},0} \\ \hat{\boldsymbol{f}}_{\mathrm{exc},1} \\ \vdots \\ \hat{\boldsymbol{f}}_{\mathrm{exc},\mathrm{m_h}} \end{bmatrix} - \begin{bmatrix} \hat{\boldsymbol{F}}_{\mathrm{nl},0}(\hat{\boldsymbol{q}}_0, \ldots, \hat{\boldsymbol{q}}_{\mathrm{m_h}}) \\ \hat{\boldsymbol{F}}_{\mathrm{nl},1}(\hat{\boldsymbol{q}}_0, \ldots, \hat{\boldsymbol{q}}_{\mathrm{m_h}}) \\ \vdots \\ \hat{\boldsymbol{F}}_{\mathrm{nl},\mathrm{m_h}}(\hat{\boldsymbol{q}}_0, \ldots, \hat{\boldsymbol{q}}_{\mathrm{m_h}}) \end{bmatrix}, \tag{29}$$

where $\mathbb{H}_{\mathrm{lin,m}} = \mathbb{K} + i(m\omega)\mathbb{D} - (m\omega)^2\mathbb{M}$ is the dynamic stiffness matrix, and the considered higher harmonics are indexed by $m = 0(1)m_h$. Each row of Eq. (29) represents an independent set of equations for an individual harmonic. However, the equations become coupled because of the nonlinear forces, which are dependent on all harmonics.
Naturally, if only the first harmonic $(m = 1)$ is considered, Eq. (29) reduces to the conventional Harmonic Balance method formulation.

6 Results

The performance of the reduction code is investigated with respect to the described shroud conditions as well as different mistuning cases. Note, that all figures are normalized by the respective eigenfreuqency and amplitude of the linear and tuned setup.
The full FE-model features $59,508$ DOFs. Linear frequency response functions (FRF) plot using rigid shroud coupling and 300 considered modal DOFs is shown in Fig. 2 on the left. The mistuning pattern, given by the frequency deviation factors of the blades with respect to the tuned blade, is presented on the right. Refering to the tuned peak at 1, which is excited by the engine order 9 [9], strong mistuning effects in the considered frequency range can be observed. Due to the mistuning other nodal diameters are excited as well and frequency splitting occurs.

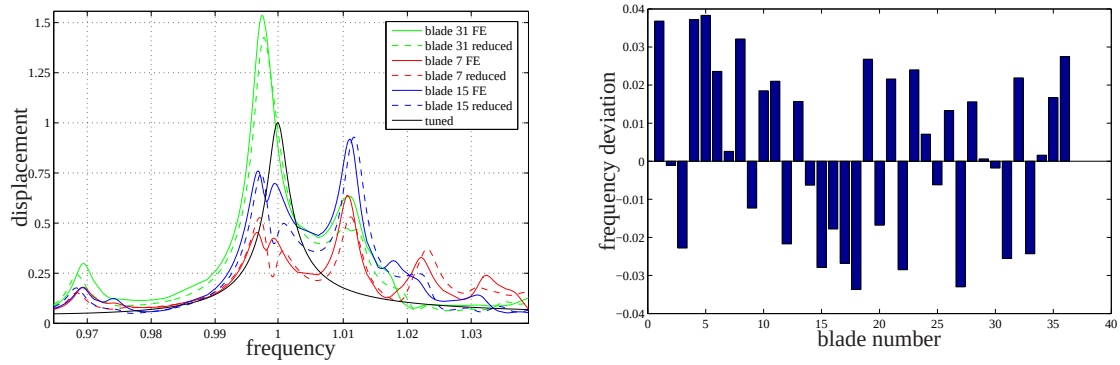

Fig. 2 Linear FRF of mistuned turbine with engine order 9 (left) and the used mistuning pattern (right).

The nonlinear analysis is usually preceded by the determination of a frequency range of interest. For this purpose a linear calculation, using the linear sliding condition, is performed to obtain a nodal diameter diagram (Fig. 3 (left)). Different normal forces are used to calculate FRFs using the HBM. It can be observed in Fig. 3 (right) that for small normal forces the nonlinear response remains very similar to the response using linear sliding. However, the behavior drastically changes, when normal forces increase. Generally, a frequency shift of the FRFs, caused by the stiffening effects in the system, can be observed. A decline of the amplitudes is apparent for $F_N \leq 5N$, because relative motion of the shrouds is still present and friction occurs. For higher normal forces ($F_N > 5N$) the amplitudes increase again, because stick becomes dominant and less energy can be dissipated by friction. Fig. 4 (left) gives a detailed representation of the nonlinear FRFs with the normal force of $F_N = 3N$. Nonlinear damping effects as well as mistuning effects can be seen. Compared to the linear case, in this particular setup both peak amplitudes in the considered frequency range are reduced by a factor of 0.4. However, compared to the tuned case, the amplitude amplification due to mistuning effects reaches a factor of 1.2 at the second peak. The global mistuned displacements at the first eigenfrequency are visualized on the right.

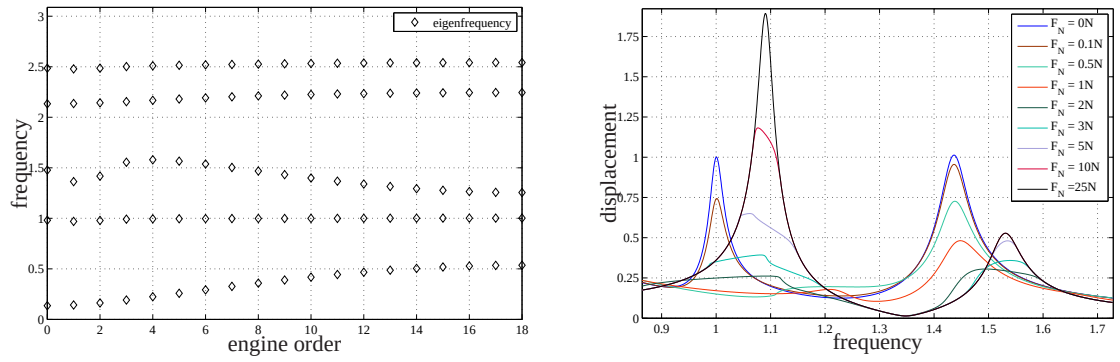

Fig. 3 Nodal diameter plot of system with sliding condition (left), Nonlinear FRF of tuned turbine with engine order 9 and different normal forces (right).

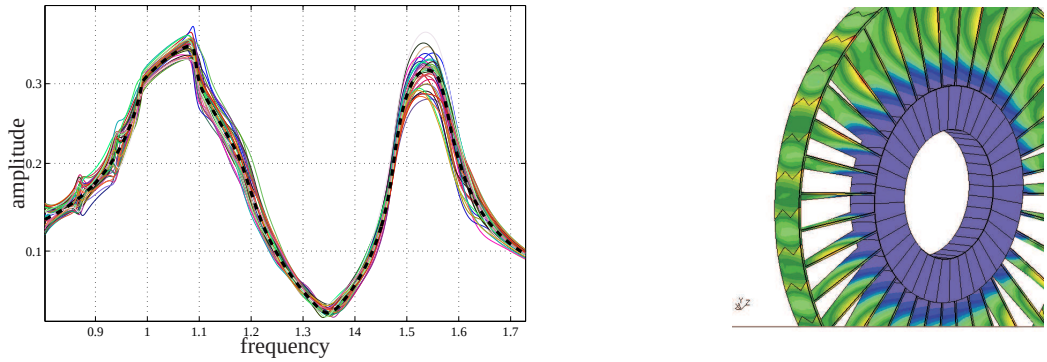

Fig. 4 Nonlinear FRF of mistuned turbine with engine order 9 and a Normal force $F_N = 2N$ (left) amplitude of the displacement at $880Hz$ (right).

7 Conclusion

In this work, a procedure to calculate nonlinear frequency response functions of mistuned turbine blades is presented. Considering constant normal forces, an approximation of the nonlinear frequency response function can be calculated very fast using the Harmonic Balance Method. Higher harmonics can be taken into account. With the presented Component Mode Synthesis the size of the system can be significantly reduced without considerable loss of accuracy.
In order to extend the contact formulation, e.g. including the possibility of varying normal forces, further friction models are to be investigated in the future.

References

1. Panning L. (2009) Systematische Verstimmung und mehrfach gekoppelte Schaufelkränze von Turbomaschinen . FVV-Abschlussbericht Nr.898, University of Hannover.
2. Hohl A., Siewert C., Panning L., Wallaschek J. (2009) A substructure based reduced order model for mistuned bladed disks. FVV-Abschlussbericht Nr.898, University of Hannover.
3. Becker J., Gaul L. (2008) CMS-Methods for Efficient Damping Prediction for Structures with Friction. Proceedings of the IMAC-XXVI, Orlando, Florida USA
4. Castanier M. P., Tan Y. Pierre C.(2001) Characteristic Constraint Modes for Component Mode Synthesis. AIAA Journal Vol. 39, No. 6
5. Lim S., Bladh R., Castanier M. P., Pierre C.(2007) Compact, generalized component mode mistuning representaion for modeling bladed disk vibration. AIAA Journal Vol. 45, No 9
6. Bograd S., Reuss P., Schmidt A., Gaul L., Mayer M. (2011) Modeling the Dynamics of Mechanical Joints. Mechanical Systems and Signal Processing, Vol. 25, Issue 8, p. 2801-2826
7. Reuss P., Zeumer B., Herrmann J., Gaul L.(2012) Consideration of Interface Damping in Dynamic Substructuring. Proceedings of the IMAC-XXX, Jacksonville, Florida USA
8. De Klerk D., Rixen D., Voormeeren S. (2008) General Framework for Dynamic Substructuring: History, Review and Classification of Techniques. AIAA Journal Vol.46 No.5 (1169-1181) doi: 10.2514/1.33274
9. Panning L. (2005) Auslegung von Reibelementen zur Schwingungsdämpfung von Turbinenschaufeln. PhD thesis, University of Hannover.
10. Voormeeren S., van der Valk P., Rixen D., (2010) Practical Aspects of Dynamic Substructuring in Wind Turbine Engineering. Proceedings of the IMAC-XXVIII, Jacksonville, Florida USA
11. Guyan R. J. (1965) Reduction of Stiffness and Mass Matrices. AIAA Journal Vol. 3, No. 2
12. Balmer B. (1993) Erhöhung der Dämpfung von Turbinenschaufeln durch Reibelemente. VDI Fortschrittberichte Serie 11, No. 197
13. Tran D.-M..(2000) Component mode synthesis methods using interface modes. Application to structures with cyclic symmetry. Computers and Structures 79